ASSESSMENT OF TEMPO-OXIDIZED CELLULOSE NANOFIBRIL INCORPORATION ON PLGA MEMBRANE CHARACTERISTICS FOR BIOMEDICAL APPLICATIONS

YUNIA DWI RAKHMATIA,* NOVITRI HASTUTI,** ISMADI,**
VITA MULYA PASSA NOVIANTI,* DEBY FAJAR MARDHIAN*** and ANDI HERMAWAN****

*Department of Prosthodontic, Faculty of Dentistry, Universitas Padjadjaran, Jl. Sekeloa Selatan I No.1,
Lebakgede, Kecamatan Coblong, Kota Bandung, Jawa Barat 40132, Indonesia

**Research Center for Biomass and Bioproducts, National Research and Innovation Agency, KST BJ
Habibie Serpong, Tangerang Selatan, Indonesia, 15314

***Department of Dental Material Sciences, Faculty of Dentistry, Universitas Padjadjaran, Jl. Sekeloa
Selatan I No.1, Lebakgede, Kecamatan Coblong, Kota Bandung, Jawa Barat 40132, Indonesia

****Laboratory of Wood Material Technology, Faculty of Agriculture, Kyushu University,
744 Motooka Nishi-ku, Fukuoka 819-0395, Japan

© Corresponding author: Y. D. Rakhmatia, rakhmatia@unpad.ac.id

Received February 26, 2025

Poly(lactic-co-glycolic) acid membranes developed for guided bone regeneration (GBR) in dental care have the shortcoming of not being rigid enough to withstand soft tissue stress during healing, which may significantly affect the bone formation process. This study aims to overcome the lack of mechanical properties of poly(lactic-co-glycolic) acid (PLGA) membranes for GBR by using cellulose nanofibers to reinforce the membranes. The manufacture of cellulose nanofibers begins with the wood pulping process of oil palm empty fruit bunches (OPEFB) residue. The fibers were then oxidized using the 2,2,6,6-tetramethylpiperidine-1-oxyl (TEMPO) system at pH 10-11 and mechanically disintegrated using ultrasonication to produce nano-sized fibers (denoted as TEMPO-oxidized cellulose nanofibers – TOCNs). The resulting TOCNs were incorporated into PLGA at concentrations of 0.4%, 0.8%, and 1.0% (wt/wt). The incorporation of TOCNs modified PLGA membranes, increasing surface texture and crystallinity, as confirmed by SEM, XRD, and FTIR. Membranes thinned with TOCNs addition, with pore size/volume peaking at 0.4% loading (6.31 nm, 0.23 cm³/g), then reverting towards neat PLGA values at 1.0%. Optimal tensile strength was noted for 0.8% TOCNs. PLGA-TOCNs composites degraded slower than neat PLGA. The research results are expected to support the use of renewable natural fibers as reinforcement for PLGA membranes. The TOCNs can effectively modify PLGA membrane properties, offering potential for tailoring these materials for biomedical applications.

Keywords: poly(lactic-co-glycolic) acid (PLGA), nanofiber, cellulose, membrane, guided bone regeneration (GBR)

INTRODUCTION

Bone and tooth injuries are the main areas of concern in tissue engineering and regenerative medicine. One of the regenerative augmentation techniques is Guided Bone Regeneration (GBR). The basic principle of GBR involves placing a mechanical barrier (membrane) to protect the blood clot and isolate the damaged bone from the surrounding connective tissue, thereby providing access to bone-forming cells to a remote space for bone regeneration. Membranes used in GBR must exhibit a combination of critical properties beyond biocompatibility to ensure successful clinical outcomes. The membrane must have

biocompatibility properties, must not affect the surrounding tissue, so that it is effective for the desired healing result and is safe for the patient.² The mechanical stability of membranes is of utmost importance because they need to maintain the regenerative space against the collapse of soft tissue.^{2,3} This is linked to the tensile strength and the tear strength of the membrane, which permit the membrane to withstand considerable forces, without the risk of rupturing.⁴ The membrane should also show controlled and predictable degradation rates, which is ideal when the membrane degrades simultaneously with the

Cellulose Chem. Technol., 59 (7-8), 825-839(2025)

newly formed bone; it should provide soft tissue an adequate amount of stability, but not too much to avoid the need for a secondary removal.5 Another membrane property is the barrier function, which is the ability of the membrane to prevent the ingress of epithelial or fibrous tissue into the bone defect site.⁶ The membrane surface features, such as topography and porosity, are also important as they regulate the diffusion of nutrients and removal of wastes, and should not allow unrestricted cell movement into the regenerative space.⁷ Considerations such as hydrophilicity must also be addressed, as it aids in promoting cell and protein adsorption, as well enhances osteoconductive functions.8 Incorporating bioactive materials into membranes, such as antibiotic treatments or growth factors, is more frequently seen in literature as a means to actively promote bone healing and stave off infection.9 Elasticity and conformability are other characteristics important of membranes; membranes must rigidly hold their barrier functions while also adapting to varying defect geometries. 10 The properties described above are necessary for next-generation GBR membranes that strive to boost regenerative activity.

Many barrier membranes have developed for clinical applications, which are classified into resorbable and non-resorbable membranes. The resorbable membrane has the advantage of being able to be absorbed by the body. In the area of GBR, resorbable membranes are increasingly favoured, as thev biodegradable and require no secondary surgical removal. The most common types of membranes include the collagen membrane, which has excellent biocompatibility, and a resorption time that aligns with the various stages of bone healing, 11 or the polycaprolactone (PCL) based membranes, which have a slower degradation rate and the potential for greater mechanical reinforcement.¹² Also, gelatin-based membranes are increasingly used due to gelatin's hydrophilic characteristics and its ability to promote cellular adhesion.13 In contrast. non-resorbable membranes require a second surgical removal because they cannot be absorbed or degraded in the body. 11 Previous studies have shown that nonresorbable titanium mesh membranes impede fibroblast cell migration in degenerative areas. 14,15 Non-resorbable membranes selected for cases requiring longer barrier function. Examples include e-PTFE membranes,

which are appreciated for their dimensional stability and cell occlusivity, ¹⁶ and titanium mesh membranes, which are superior in mechanical strength and keep space in large defect reconstructions. ^{17,18} Additionally, some innovations like membranes made of magnesium based alloys, which slowly degrade over time with a low inflammatory reaction. ¹⁹ Thus, GBR membranes are changing over time, as they need to be adapted to the clinical requirements and concerns like the dimensions of the defect, the expected time of healing, and the patient.

Currently, the most widely used polymer in the development of resorbable membranes in GBR is poly(lactic-co-glycolic) acid (PLGA). PLGAbased membranes have been approved by the Food and Drug Administration (FDA) for biomedical applications.²⁰ However. membranes have unsatisfactory mechanical properties. The PLGA membrane is not rigid enough to withstand soft tissue stress during healing. its degradation process so unpredictable, which significantly affects the bone formation process. The results of a previous study showed a fluvastatin-loaded degradable PLGA membrane for GBR, only effective for minimal bone formation under the PLGA membrane.21

In addition to the widely researched PLGA, various other polymers have emerged as promising options for GBR, each with unique mechanical, biological, and degradation properties that meet requirements. Polycaprolactone clinical received considerable attention due to its strong mechanical properties and prolonged degradation timeline, which is beneficial for extended bone periods; when regeneration combined with hydroxyapatite, it notably improves osteoconductivity and maintains space over time. 12 Chitosan, a natural polymer, is recognized for its antimicrobial effects and compatibility with biological tissues; its application in electrospun membranes promotes cell adhesion and growth, making suitable for **GBR** purposes.5 Polydioxanone (PDS), a synthetic and absorbable polymer with a moderate degradation rate, has been effectively utilized in barrier membranes due to its significant initial mechanical strength consistent degradation pattern, minimizing the likelihood of early collapse.²² Another significant option is polyurethane (PU), which allows for precise adjustments of elasticity and degradation through chemical methods, resulting

customizable scaffolds with improved angiogenic properties.³ Gelatin, derived from collagen, is frequently combined with synthetic polymers like PCL to improve biocompatibility and manage degradation rates while facilitating osteogenesis.⁴ In addition, silk fibroin has been recognized for its remarkable tensile strength slow and biodegradation, which aids in cellular infiltration and blood vessel formation in GBR applications.⁷ Although polyethylene glycol (PEG) is highly hydrophilic and degrades quickly, it is often chemically altered or blended to overcome its mechanical limitations, allowing its application in GBR scaffolds compatible with soft tissues.²³ Lastly, polyvinyl alcohol (PVA) has shown encouraging barrier properties and compatibility with cells, often serving as a matrix for delivering bioactive substances in GBR systems.8 These developments in polymeric materials for GBR highlight a move towards multifunctional scaffolds that integrate bioactivity, mechanical support, and biodegradability in a manner adaptable to clinical needs.

Cellulose nanofibers are nanomaterials derived from a saccharide polymer (polysaccharide) called cellulose. The addition of nanocellulose from oil palm empty fruit bunches (OPEFB) to the polymeric membrane poly(methyl vinyl ether-comaleic acid)-poly(ethylene glycol) showed an increase in the mechanical properties of the membrane and the elasticity of the membrane only with the addition of 5% cellulose nanofibers.²⁴ Although the crystallinity of cellulose nanofibers is suspected to be the main factor determining their mechanical properties, the crystalline nature of cellulose does not prevent it from being degraded.²⁵ Softwood nanofibers obtained from the oxidation of 2,2,6,6-tetramethylpiperidine-1-oxyl (TEMPO) are known to have a crystallinity index of up to 74%, with a uniform diameter of 3-4 nm and a fiber length of 1 micron.²⁶ Our previous research in the extraction of cellulose nanofibers from OPEFB using TEMPO-mediated oxidation showed that the resulting nanofibers had thermal resistance and crystallinity of up to 55%.²⁴ The crystallinity index of cellulose nanofibers determines its mechanical properties and heat resistance. Thus, cellulose nanofibers can be used as a reinforcement to improve the properties of membrane composites.

Cellulose nanofibers (CNFs) obtained from OPEFB have distinct advantages compared to CNFs sourced from traditional materials, such as wood, cotton, or bacterial cellulose. CNFs derived

OPEFB provide a sustainable environmentally friendly option by transforming a plentiful agricultural waste into a valuable resource, promotes zero-waste initiatives alleviates the environmental impact associated with the palm oil industry.²⁷ They are notably costeffective since OPEFB is an abundant byproduct, making the production of CNFs economically beneficial in regions that cultivate palm oil.²⁸ The moderate crystallinity index of OPEFB CNFs (~55%) enhances their process ability and versatility, striking a balance between mechanical thermal stability, and controlled strength, biodegradability that is ideal for biomedical uses.²⁹ The chemical reactivity of OPEFB fibers is improved due to the presence of surface hydroxyl facilitating straightforward chemical modifications for advanced applications, such as biosorbents and biomedical membranes.³⁰ In addition, leveraging local resources supports the establishment of domestic CNF industries, decreasing dependence on wood-derived CNFs that are generally imported from suppliers outside the region.³¹

The production of resorbable PLGA membranes for clinical uses in dental bone treatment is still primarily conducted overseas. Therefore, it is essential to develop technology for creating PLGAbased resorbable membranes reinforced with cellulose nanofibers to enhance their application in GBR within the medical field. Specifically, it is anticipated that the inclusion of CNFs will considerably enhance the mechanical strength, elasticity, and thermal stability of the PLGA membranes. These enhancements are due to the unique characteristics of CNFs, including their nanoscale size, high aspect ratio, and crystalline structure. Despite cellulose being biodegradable, the crystallinity index of the nanofibers, which has previously achieved up to 55% through TEMPOmediated oxidation of OPEFB, offers a robust nanofibrillar network that serves as a reinforcing structure within the polymer matrix. This structural reinforcement boosts load-bearing capacity and stability without sacrificing the degradability that is crucial for resorbable membranes. The choice of OPEFB as a raw material is deliberate as it is plentiful, being an agricultural waste product in regions that produce palm oil, thus providing a cost-effective and sustainable source nanocellulose. Additionally, utilizing this biomass helps to mitigate the environmental issues related to OPEFB disposal. In this regard, developing PLGA-

CNF composite membranes with local resources like OPEFB not only aims to substitute imported commercial membranes, but also strives to produce with enhanced biomechanical membranes properties, optimized degradation profiles, and surface modifications potential that antimicrobial or bioactive, which are vital for effective space maintenance and guided bone regeneration. Therefore, this research aims to analyze the characteristics of PLGA membranes supported by nanocellulose sourced from OPEFB and to assess the impact on enhancing the properties of the PLGA membranes. The study will assessing the mechanical. concentrate on morphological, and degradation characteristics of the developed membranes to confirm their clinical applicability.

EXPERIMENTAL

Materials

Raw and bleached Kraft pulp of OPEFB was kindly supplied by the Research Center for Biomass and Bioproducts, National Research and Innovation Agency (Cibinong, Indonesia). Ethanol, poly(lacticco-glycolic) acid (PLGA) and 2,2,6,6tetramethylpiperidine-1-oxyl (TEMPO) were purchased from Sigma Aldrich (Singapore); 1.4 dioxane, sodium bromide (NaBr), sodium hydroxide (NaOH) and sodium borohydride (NaBH₄) were purchased from Loba Chemie (Mumbai, India). Sodium hypochlorite (NaClO) (10% concentration) was purchased from Bratachem Chemical Company, Bogor, Indonesia. All reagents were used without any further purification. The water used in this study was deionized water (DI). Saline solutions (0.9% NaCl) were bought from Otsuka, PT Widatra Bhakti, Indonesia.

Preparation of TOCNs

The mechanical pre-processing of raw OPEFB pulp begins with washing, drying, and mechanical grinding to reduce size and eliminate residual oil and debris. This is followed by an alkaline treatment, or delignification, where the ground fibers are treated with a sodium hydroxide (NaOH) solution, typically at concentrations of 2-10%, and heated to 80-100 °C. This step removes lignin and hemicelluloses, leaving behind primarily cellulose fibers. An optional but common bleaching step may then be applied using agents, such as sodium hypochlorite (NaOCl) or hydrogen peroxide (H2O2), to further purify the cellulose and remove any remaining lignin. While similar to commercial bleached Kraft pulp production, this process generally results in slightly less refined cellulose. In some protocols, mechanical refining through high-speed blending or milling is performed to enhance fiber fibrillation before oxidation. Finally, the resulting bleached Kraft pulp can either be dried for storage or directly subjected to TEMPO-mediated oxidation to produce OPEFB derived TEMPO-oxidized cellulose nanofibers (TOCNs).

In this study, the bleached Kraft pulp of OPEFB was soaked in a 0.01 M HCl solution for 30 min for demineralization. TOCNs were prepared by the TEMPO/NaBr/NaClO system at pH 10 according to our prior study.32 In brief, a 2.5 g of dry weight of demineralized Kraft pulp (about 85% of cellulose content) was suspended in water (250 mL) containing TEMPO (16 mg/g cellulose) and NaBr (100 mg/g cellulose). The oxidation reaction was initiated by adding 1.7 M NaClO aq as oxidant. The pH of the suspension was maintained at 10 by adding 0.5 M aqueous NaOH during the reaction. After 2 h, the reaction was quenched by adding ethanol (2 mL), followed by the addition of NaBH₄ (100 mg/g cellulose), and the resultant mixture was further stirred for 1 h. The obtained suspension was thoroughly washed using deionized water by centrifugation in 3500 rpm for 10 minutes and then sonicated by an ultrasonic homogenizer for 30 min by applying the "on and off" method ("on" for 5 minutes, then "off" for 3 minutes). The obtained TOCNs were kept at 4 °C until further use. The morphological appearance of the raw pulp, the bleached Kraft pulp, TOCNs in aqueous solution, and TOCNs after freeze drying is shown in Figure 1.









Figure 1: Morphological appearance of (a) raw OPEFB pulp, (b) bleached Kraft OPEFB pulp, (c) OPEFB TOCNs in aqueous solution, and (d) OPEFB TOCNs after freeze drying

Preparation of PLGA-TOCNs

About 100 mg of PLGA was dissolved in 5 mL of 1.4-dioxane and stirred at 60 °C for 20 minutes. The solution of TOCNs, with the concentration of 1%, 0.8%, and 0.4% (w/v), was added into the respective PLGA-1,4-dioxane solutions and stirred until well dissolved. The solutions then were homogenized under sonication with the output voltage of 24 V for 2-3 minutes. The solutions were then poured into a mold and dried at room temperature for 72 hours. The notation of the respective membranes was done in accordance with the amount of nanocellulose added, as follows: PLGA-TOCNs 0.4% (0.4); PLGA-TOCNs 0.8% (0.8); PLGA-TOCNs 1% (1). A PLGA only membrane was also prepared as a control (0).

Thickness and porosity measurement

The thickness of each membrane was measured with a micrometer under no pressure at four random locations on each membrane sample, and the mean was calculated. Then, pore volume and pore size distribution were assessed using the Brunauer–Emmett–Teller (BET) technique, which was applied to nitrogen adsorption–desorption isotherms. The evaluation took place at 77 K, using a surface area and porosity analyzer (Surface Area and Pore Analyzer Micromeritics Tristar II Plus 3020, Micromeritics Inc., Georgia, USA). Before the analysis, the samples were degassed under vacuum at 100 °C for 12 hours to eliminate moisture and gases.

Scanning electron microscopy (SEM)

The morphology of raw pulp, TOCNs, and PLGA-TOCNs membranes were observed on a scanning electron microscope (Zeiss Type EVO 50, Germany) equipped with a navigation camera at the Centre for Standardization of Sustainable Forest Management Instrument of Agency of Instrument Standardization, Ministry of Environment and Forestry, Bogor, Indonesia. PLGA and PLGA-TOCNs samples were mounted on carbon tape without any coating, and observed at an accelerating voltage of 10 kV.

Transmission electron microscopy (TEM)

The length and width of TOCNs were measured by a transmission electron microscopy (TEM) (JEM 2100-HC, JEOL Ltd., Tokyo, Japan). The TEM equipment operated at an accelerating voltage of 120 kV, as mentioned in a previous study.³³ A 5-µL sample of NS suspension (0.1% concentration) was applied onto a TEM grid coated with carbon. Subsequently, a drop of sodium phosphotungstate solution (1% weight/volume) was added before the sample was dried. The excess liquid was eliminated using filter paper. Subsequently, the grids were subjected to vacuum drying for a duration of 30 minutes. The length of 50 individual crystals was quantified using image processing software (Image-J version 1.51s) on TEM images.

X-ray diffraction (XRD)

X-ray diffraction (XRD) data were recorded on a Shimadzu X-ray diffractometer (XRD 7000) operated at 40 kV and 30 mA. The specimens were scanned stepwise over the scattering angle (20) range from 5° to 40°, at a scanning speed of $0.6^{\circ}/\text{min}$ with CuKa radiation ($\lambda = 1.541$). The crystallinity index, CrI (%), was calculated using the method reported by Segal *et al.*³⁴

Fourier transform infrared spectroscopy (FTIR)

FTIR spectra were recorded on a spectrophotometer. Prior to analysis, a 100 mg portion of the sample was ground and mixed with 5 mg of KBr. The resulting mixture was pressed into transparent pellets and analyzed in the spectral range of 400-4000 cm⁻¹ with a resolution of 2 cm⁻¹ for each sample.

Mechanical testing

The mechanical properties of the membranes were evaluated to measure the stress–strain value, the tensile strength, and the elastic modulus of experimental membranes using a universal testing machine (AG-IS, Shimadzu, Kyoto, Japan). Membrane specimens, with the size of 20×25 mm, were prepared and attached to holders, equipped with a 50 kgf load cell and a crosshead speed of 50 mm/min.

pH measurement and degradation rate

Membranes with a diameter of 8 mm were suspended in 50 mL of saline solution in conical tubes at a pH of 7.4 and 37 °C. Slight changes in the pH of the solution containing the membranes were measured every 7 days using a pH meter. Each type of experimental membrane was replicated three times. Each membrane was kept in a 50 mL saline solution (Otsuka, Jakarta, Indonesia) at 37 °C and was monitored to evaluate its degradation rate. Each sample was weighed and the result was recorded before being placed back into the PBS solutions during 4 weeks. The samples were removed, rinsed with distilled water, dried at room temperature and their dry mass was weighed with an analytical balance. The degradation rate was measured and statistical analysis was carried out by one way ANOVA, with post hoc Tukey test at p<0.05.

RESULTS AND DISCUSSION Macroscopic analysis

Macroscopic images provide a qualitative assessment of the impact of TOCNs incorporation into the PLGA membrane on its surface morphology (Fig. 2). The surface of the neat PLGA appears smooth, uniform, with minimal visible texture and porosity. There are no noticeable patterns or irregularities. This is consistent with the typical characteristics of PLGA membranes prepared via solvent casting or similar methods. Previous studies have also reported similar smooth

surfaces for neat PLGA membranes.³⁵ This characteristic smoothness can be attributed to the inherent properties of PLGA during the membrane formation process, where the polymer chains arrange themselves to minimize surface energy.

The incorporation of TOCNs (TEMPO-oxidized cellulose nanocrystals) tends to cause a slight increase in surface texture, characterized by faint, small-scale roughness or fine granularity. The surface of PLGA-TOCNs 0.4 becomes slightly more textured, but still relatively uniform. Sample PLGA-TOCNs 0.8 shows a more pronounced texture, with visible concentric or directional patterns forming across the surface. This suggests a transition towards a more structured or processed texture. The surface of PLGA-TOCNs 1.0 no longer exhibits uniformity, indicating significant

surface modification or structural changes. Similar observations have been reported in other polymernanoparticle composite systems, where the presence of nanoparticles introduces surface roughness.³⁶ The increased roughness and pattern formation could potentially influence membrane's surface area and wettability, impacting its interaction with the surrounding environment. Research on similar nanocomposite films suggests that increased nanoparticle concentration can lead to aggregation and pattern formation.³⁷ The observed changes of PLGA-TOCNs 1.0 are consistent with studies showing that high concentrations of nanoparticles in polymer composites can lead to instability and non-uniformity.³⁸

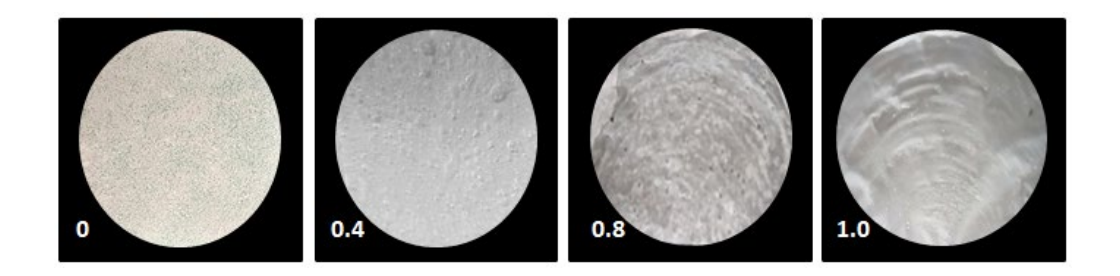


Figure 2: Neat PLGA (0) and PLGA-TOCNs (0.4, 0.8, 1.0%) samples

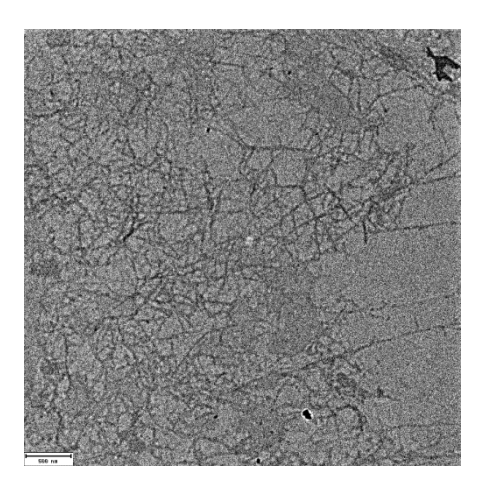


Figure 3: TEM image of OPEFB-TOCNs (scale bar: 500 nm)

TEM analysis

To further demonstrate the size of the fibrillated raw pulp of OPEFB fibers, TEM analysis was performed. The results of the TEM analysis are shown in Figure 3. TEM examinations revealed that the raw pulp treatment, employing TEMPO-mediated oxidation and mechanical disintegration

through sonication, effectively reduced the size of the fibers. Transmission Electron Microscopy (TEM) analysis reveals nanoscale dimensions in OPEFB fibers, as shown in Figure 3. However, the staining techniques used in TEM can affect the perceived size, potentially widening the image during analysis. This approach is particularly effective in characterizing mesoporous structures, defined by pore diameters ranging from 2 to 50 nm.³⁹

The efficacy of mechanical treatment in disrupting the association of microfibrils relies on the arrangement of microfibrils in the original tissue. Nevertheless, in the absence of oxidation, the microfibrils failed to disperse in water alone through mechanical treatment. Hence, TEMPOmediated oxidation effectively facilitates the disintegration process by weakening the adhesion between microfibrils and promoting electrostatic repulsion between them, resulting in introduction of substantial quantities of carboxylate groups. 5,22 Similarly to the previous research by Kong et al., 40 this TEM image demonstrate that the utilization of TEMPO in the oxidation process leads to the transformation of a significant portion of raw pulp of OPEFB fibers into separate

nanofibers, characterized by a nearly consistent width of 3-4 nm and a length of several microns. Consequently, this results in an increased aspect ratio.³

SEM images

Surface morphology images of the membranes are provided in Figure 4. The morphological changes from the original OPEFB fiber to the TOCNs obtained from this material can be observed. The initial pulp revealed that the combination of TEMPO-mediated oxidation conducted at pH 10-11 and ultrasonication effectively produced nanofibrillated fibers from the OPEFB pulp. These results are in good accordance with those of the previous study, where TEMPO-mediated oxidation was performed at pH 10 and 6.8.⁴¹

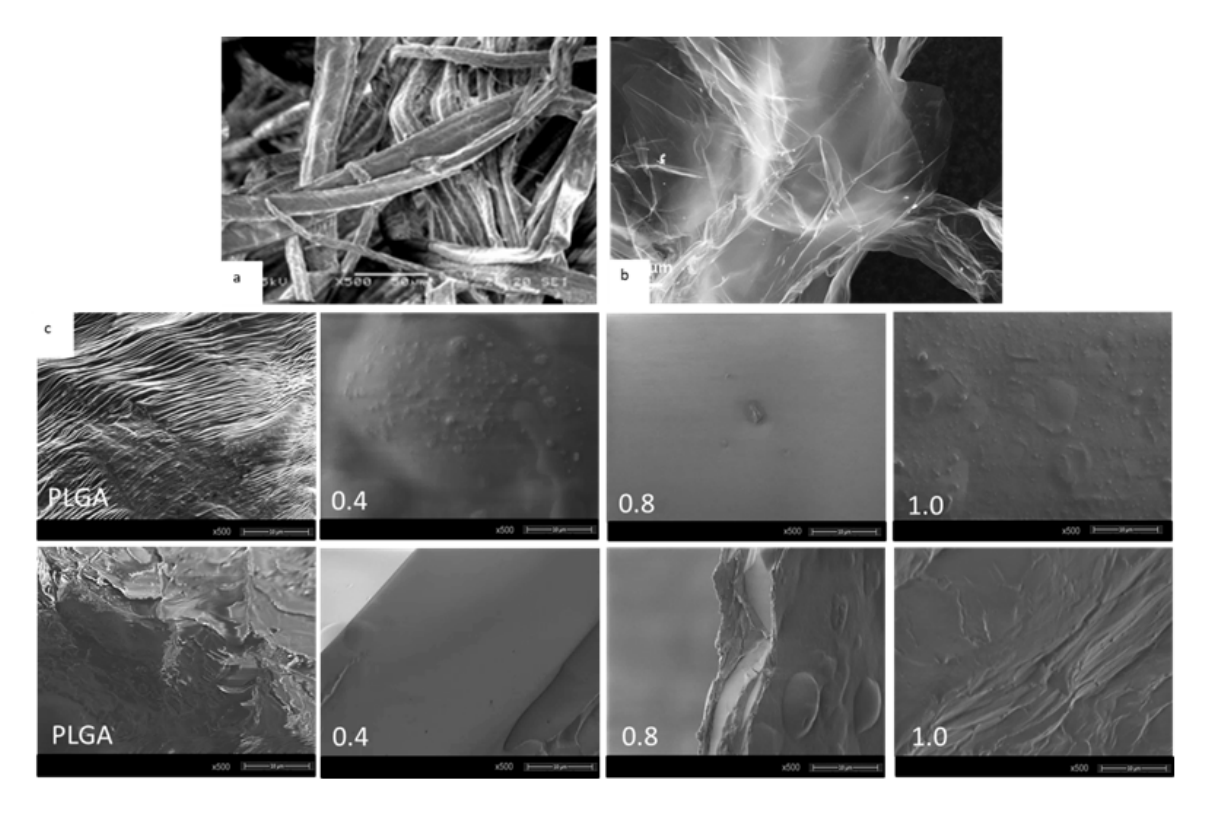


Figure 4: SEM images of a) raw pulp, b) TOCNs, c) Surface (upper) and cross-section (lower) topography of PLGA-TOCNs membrane samples 0, 0.4, 0.8, 1.0% (scale bar: 10 μm, magnification: 500×)

In addition, the polymeric matrix was supplemented with TOCNs of different lengths, constituting a concentration of 5 wt%. Figure 4 (a and b) reveals a significant change in the size of fibers, from the large OPEFB fibers to much smaller and fine fibers, indicating successful

defibrillation. This led to the formation of membranes with slightly different properties. Utilizing longer TOCNs can lead to improved transparency, thermal conductivity, and mechanical characteristics.¹⁰

Figure 4 (c) shows the surface and cross-section topography of PLGA and **PLGA-TOCNs** membranes. The PLGA-only membranes show smooth, homogenous, and compact surfaces, with ridges or directional textures, both on the surface and in cross-section. The typical SEM morphology of these membranes prepared via solvent casting show the ridges or directional textures, which likely arose from the solvent evaporation process during membrane formation, leading to preferential alignment of the polymer chains. These features suggest a dense and well-packed polymer structure.¹⁵ The SEM of PLGA-TOCNs 0.4 shows moderately smooth, showing a less fibrous structure or visible layered features, compared to PLGA.

The surface of PLGA-TOCNs 0.8 becomes rougher and appears more heterogeneous, with visible pits and depressions. The cross-section topography reveals a fibrous or layered internal structure. The surface of PLGA-TOCNs 1.0 exhibits significant roughness with distinct pits and craters, compared to other PLGA-TOCNs membranes. Fibrous features dominate the structure, with an irregular surface, compared to other samples. The presence of 1% TOCNs enhanced the visibility of the fibrous structure in the membranes.

This suggests that at this higher concentration, the TOCNs significantly disrupt the PLGA matrix, leading to substantial changes in the membrane morphology. The pits and craters could be attributed to the aggregation of TOCNs, phase separation between the PLGA and TOCNs, or the formation of voids during drying. The dominant fibrous features indicate that the TOCNs network becomes more interconnected and pronounced at this concentration. This significant change in morphology could drastically affect the membrane's mechanical properties, permeability, and

degradation rate. In line with this, a previous study revealed that the incorporation of TOCNs into an alginate polymeric membrane resulted in a decrease in membrane shrinkage and a reduction in the groove-like structure of the membrane.⁴²

The integration of TOCNs into the PLGA matrix results in two distinct yet complementary impacts on the surface of the membrane, depending on the observation scale. On a macroscopic scale, the membranes show a slight increase in surface texture, appearing as fine granularity. This effect arises from the physical incorporation of nanofibers within the PLGA matrix, potentially enhancing the surface area. On the microscopic scale, as observed by SEM, the nanofibers help create a more uniform and continuous surface morphology, likely due to better compatibility and dispersion of TOCNs within the PLGA polymer, which could be beneficial for biological interactions, such as cell attachment and proliferation.

XRD analysis

Figure 5 illustrates the XRD patterns for raw pulp of OPEFB, TOCNs, PLGA, and TOCNs-PLGA membranes. The TOCNs clearly had the crystal structure of cellulose I, whose crystallinity index and crystal size on the [100] plane were almost equal to those of the original OPEFB pulp. The crystallinity index (Cr.I.) dropped from 61% in raw pulp to 46% in TOCNs, suggesting partial disruption of crystalline regions due to surface oxidation.⁴³ Moreover, the crystal width on the (200) plane (\sim 22.5° 20) exhibited a slight reduction after oxidation, although the cellulose I structure remained preserved.⁴⁴ These findings demonstrate that oxidation primarily impacts the surface and disordered areas of the cellulose microfibrils, where sodium carboxylate groups are introduced, without undermining the overall crystalline framework.¹²

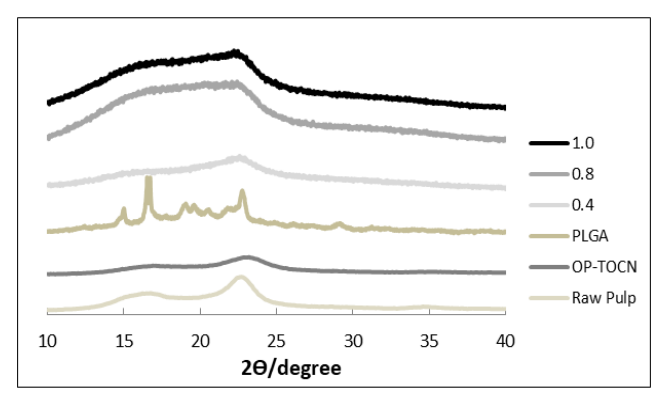


Figure 5: XRD patterns of raw pulp, TOCNs, PLGA, and PLGA-TOCNs of 0.4, 0.8, 1.0%

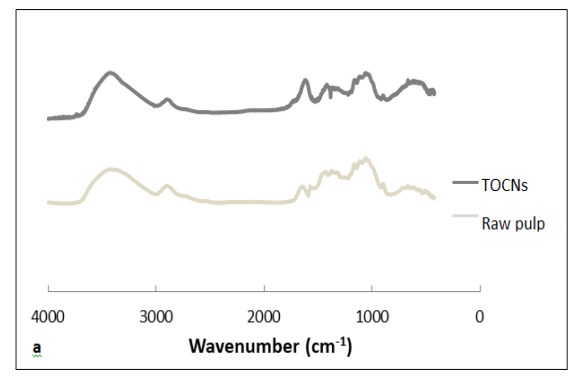
The XRD curves of raw OPEFB pulp and TOCNs reveal that the oxidation procedure employing TEMPO successfully preserves the crystalline structure of cellulose. The diffraction peaks for both the raw pulp and TOCNs display typical characteristics of cellulose I, with notable reflections at about $2\theta = 15.4^{\circ}$ and 22.6° , corresponding to the (101) and (002) planes, respectively. 45 This observation confirms that the TEMPO-mediated oxidation maintained cellulose I crystalline structure, consistent with earlier studies.^{8,12} The findings indicated that the TEMPO oxidation reaction occurred on the surface of cellulose, without affecting the crystal structure. 5,26,46 This is an important revelation, as preserving the crystallinity of nanocellulose is generally beneficial for improving the mechanical characteristics of composite materials.

In contrast to TOCNs, the XRD pattern of neat PLGA shows a broad amorphous halo instead of distinct crystalline peaks, indicative of its randomly distributed copolymeric lactic and glycolic acid structure, preventing efficient packing and longrange order.^{24,47} The amorphous nature of PLGA contributes to its flexibility and biodegradability. On the other hand, when TOCNs are added at concentrations of 0.4%, 0.8%, and 1%, a gradual increase in crystallinity is noted in the composite membranes compared to the neat PLGA. This improvement is linked to the nucleation effect of TOCNs, which offer a structured surface that encourages partial alignment and crystallization of adjacent PLGA chains. The TOCNs may serve as a template, aiding the arrangement of PLGA segments and resulting in better structural organization within the polymer matrix.²⁵

FTIR analysis

Figure 6 displays the FTIR spectra differentiating between the raw OPEFB pulp and

TOCNs, which confirms the chemical alterations resulting from the TEMPO-mediated oxidation and the following nanofibrillation procedures. The pronounced peak around 1618 cm⁻¹, related to the stretching vibration of asymmetric carboxylate $(-COO^{-}),$ indicates the transformation of cellulose hydroxyl groups into carboxylate functionalities on the surface of the nanocellulose. This specific peak, which is absent in the OPEFB raw pulp, strongly signifies the oxidative transformation of cellulose hydroxyl groups into carboxyl groups - a crucial chemical modification linked with TEMPO oxidation, 48,49 similar spectral indicators confirmed oxidation effectiveness in nanocellulose derived from lignocellulosic biomass. The existence of a minor shoulder at approximately 1734 cm⁻¹ in the TOCNs sample implies that some trace lignin remains, likely due to incomplete removal of lignin or residual ester linkages. Previous studies have documented similar shoulders in TEMPO-oxidized celluloses, attributing them to minor carbonyl groups from leftover lignin or hemicellulose derivatives. 32,50,51 Additionally, the diminished intensity at 1517 cm⁻¹, which corresponds to the aromatic C-O stretching mode associated with the guaiacol rings of lignin, confirms substantial lignin removal from the pulp during the oxidation process.⁵² This observation aligns with findings by Raju et al., 49 who noted that reduced aromatic peak intensities correlate directly with effective lignin extraction from steam-exploded and oxidized cellulose fibers. Collectively, these spectral features suggest that, while TEMPO oxidation effectively introduces carboxyl functionalities, essential for the dispersion of nanofibrils and surface charge, the procedure may leave trace amounts of lignin, influencing the thermal stability and hydrophilicity of TOCNs.



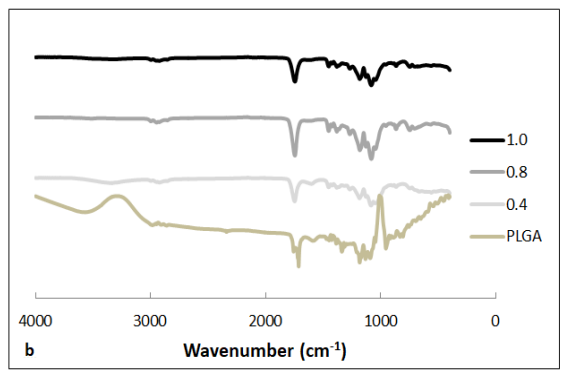


Figure 6: FTIR spectra of (a) raw pulp and TOCNs; (b) PLGA and PLGA-TOCNs 0.4, 0.8, and 1.0%

The presence of this residual lignin, indicated by minor peaks, has been highlighted in valorization studies of OPEFB fibers, underscoring the difficulty in achieving complete delignification during the production of green nanocellulose.⁴⁸ modifications improve chemical hydrophilicity and reactivity of the resulting nanofibrils, which are vital for future functional applications. Recent analyses also suggest that residual lignin provides beneficial UV resistance and antioxidant properties, potentially increasing the material's value for applications.⁵¹ As a result, the FTIR spectra shown in Figure 6 not only confirm the successful oxidation functionalization of cellulose, but also present essential evidence of lignin retention – an important consideration for the ultimate use of the material.

The FTIR spectra of PLGA display distinctive peaks indicative of ester functional groups and aliphatic C-H stretches, which are key identifiers of its chemical composition. Notably, the sharp absorption peak located between 1750 and 1745 cm⁻¹ is associated with the C=O stretching vibrations of ester bonds, as consistently found in structural analyses of PLGA biopolymers. 53,54 Furthermore, the aliphatic C-H stretching vibrations generally fall within the range of 2990 to 2940 cm⁻¹, which is attributed to the asymmetric and symmetric stretching modes of methyl and methylene groups present in the polymer chains. 55,56 These reference peaks act as benchmarks for evaluating any structural changes when PLGA interacts with reinforcing nanofibers, such as TOCNs. With the addition of TEMPO-oxidized cellulose nanofibrils, notable spectral changes occur, particularly the heightened O-H stretching bands found between 3600 and 3000 cm⁻¹, indicating hydroxyl groups introduced by TOCNs and their hydrogen bonding capacity with the ester linkages in PLGA.^{57,58} At the same time, the absorption band in the range of 1200 to 1000 cm⁻¹, related to C–O stretching vibrations of ester bonds and possible contributions from carboxylates, becomes more pronounced, signaling synergistic chemical interactions between PLGA TOCNs.59

The FTIR spectra of the PLGA membrane combined with different concentrations of TOCNs display important chemical interactions, especially visible in the absorption range of 1600 to 1640 cm⁻¹, where a distinct and amplified peak is noted, particularly in the 0.4% PLGA-TOCNs sample. This peak is linked to C=O stretching

vibrations, mainly due to ester functionalities associated with PLGA, but its increased intensity indicates contributions from the carboxylate groups in TOCNs and possible hydrogen bonding interactions at the interface between the polymer and filler. Recent research confirms that C=O stretching in this region functions as a sensitive marker for polymer-nanofiber interactions, such through mechanisms particularly hydrogen bonding and electrostatic interactions. 54,60 This spectral behavior implies incomplete hydrogen bonding saturation at moderate TOCN concentrations, resulting in functional groups still available for identification. At higher TOCN concentrations (0.8%-1%), a reduction in the intensity of this peak suggests that available hydrogen bonding sites are saturated, leading to more integrated molecular interactions within the composite matrix, aligning with observations by Tuanchai et al. and Bukhari et al.57,58 These findings, when analyzed alongside characteristic ester (1750 cm⁻¹) and aliphatic C-H (2990-2940 cm⁻¹) absorptions, provide strong evidence of structural and modifications essential interfacial composite's functional attributes. Concurrently, the region around 1200 to 1000 cm⁻¹, representing C=O stretching vibrations originating from both PLGA ester groups and the carboxylate functionalities of TOCNs, displays heightened intensity, suggesting overlapping chemical influences from both materials and confirming successful blending.⁶¹ This spectral behavior corroborates previous studies where cellulose nanofibers enhance interfacial compatibility within hydrophobic matrices like PLGA, driven by interactions such as hydrogen group engagement.55 polar bonding and Importantly, the shifts and changes in intensity of both hydroxyl and carbonyl absorption bands highlight improved molecular interactions at the composite interface, indicating better dispersion and interfacial adhesion.⁶² The intensified peak observed in the FTIR spectra of PLGA/TOCNs composite is found around 1030-1050 cm⁻¹, which is associated with the C-O-C stretching vibration of cellulose nanofibrils present in TOCNs. The increase in intensity of this peak, when compared to pure PLGA, suggests that TOCNs have been successfully integrated and are interacting within the PLGA matrix.44,63 Furthermore, this interaction could involve hydrogen bonding between the hydroxyl and carboxyl groups of TOCNs and the ester groups of PLGA, slightly modifying the vibrational environment and thereby enhancing the peak's intensity. These structural alterations impact physicochemical directly the characteristics of the material, as noted in surface-modified PLGA composites designed for biomedical scaffold applications.⁶¹ Therefore, the alterations observed in the FTIR spectra reinforce the incorporation of TOCNs and the chemical synergy at the interfacial level within the PLGA network, resulting in enhanced composite stability and performance.

Thickness and pore size measurement

The average thickness of the PLGA-only membrane was found to be 1.12 mm, which is significantly thicker compared to the PLGA-TOCNs 0.4, 0.8, and 1.0 membranes, with respective thicknesses of 0.08 mm, 0.10 mm, and 0.19 mm (Table 1). This decrease in thickness with the incorporation of TOCNs indicates an improvement in porosity and a restructuring of the matrix.

The pore measurement data from Table 1 provides valuable insights into the relationship

between the membrane's microstructure and its mechanical properties. The PLGA-TOCNs 0.4 membrane exhibits the highest pore volume (0.23 cm³/g) and a significantly larger average pore diameter (6.31 nm) compared to the other membranes, which are beneficial for promoting cell infiltration, nutrient exchange, and waste removal, though these characteristics might also create points of stress concentration that could weaken tensile strength. In addition, the inclusion of TOCNs led to an increase in pore size and volume, with measurements ranging from 3.23 to 6.31 nm, which corresponds to the mesoporous classification set by IUPAC (2-50 nm). 42,63-65 These modifications are attributed to cross-linking interactions between the carboxylate groups present in TOCNs and the PLGA chains, which enhance porosity and may be beneficial for the penetration, migration and the proliferation of cells. In addition, the higher pore volume of PLGA-TOCNs membranes indicate an interconnected porous structure of the membranes, which is advantageous in terms of transporting nutrients and waste products of cell metabolism.⁴⁵ However, the larger pores may act as stress concentration points, leading to premature failure under tensile loading.

Table 1
Average of pore measurements of PLGA-TOCNs membranes

Samples	Thickness (mm)	Average pore size distribution (nm)*	Average pore volume $(cm^3/g)^*$
PLGA	1.12	3.01	0.02
PLGA-TOCNs 0.4	0.08	6.31	0.23
PLGA-TOCNs 0.8	0.10	4.86	0.03
PLGA-TOCNs 1.0	0.19	3.23	0.06

^{*} Pore size and pore volume were measured based on BET method

Mechanical tests

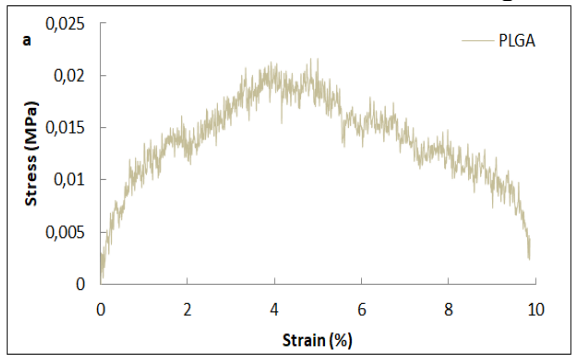
The membrane composed solely of PLGA demonstrates a significantly lower tensile strength when compared to those made from PLGA-TOCNs (Fig. 7). After the peak stress, the PLGA membrane experiences a significant decline in stress, indicating failure or degradation of the material. The PLGA only membrane exhibits a very low Young's modulus, of approximately 0.002 MPa, reflecting limited stiffness and flexibility, with an extended strain range of about 10%. On the other hand, PLGA generally has a Young's modulus that lies between 1.4–2.8 GPa, influenced by its lactic/glycolic ratio and molecular weight.⁵³ This suggests that the pure PLGA material is relatively

fragile and susceptible to breaking under tensile forces.

Generally, adding TOCNs improves the tensile strength of the PLGA membranes, highlighting the reinforcing properties of the nanocellulose. Sample **PLGA-TOCNs** shows significant 0.4 a enhancement in modulus, achieving around 0.6–0.8 MPa. Membrane PLGA-TOCNs 0.8 highlights additional improvement, with modulus values nearing 1.2-1.5 MPa. Meanwhile, PLGA-TOCNs 1.0 reaches the highest mechanical performance, with Young's modulus close to 1.8-2.0 MPa. This pattern illustrates a direct relationship between the concentration of TOCNs and the stiffness of the material, which can be attributed to strong interfacial interactions and hydrogen bonding between the cellulose nanofibers and the PLGA matrix. The increase in mechanical strength is also a result of the high intrinsic stiffness of TOCNs (about 110–150 GPa), which serve as efficient reinforcing fillers. ^{26,65} The data also indicates that the membrane stiffness increases slightly with the addition of TOCNs. The increased stiffness could be attributed to the high Young's modulus of cellulose, which is significantly higher than that of PLGA. ³⁷ The TOCNs nanofibers effectively stiffen the PLGA matrix, making the composite membrane more resistant to deformation under stress.

The tensile strength of PLGA-TOCNs decreases as the additive concentration increases. Among the

PLGA-TOCNs samples, the optimal concentration for tensile strength is 0.8% TOCNs. This implies that at this concentration, the TOCNs nanofibers are adequately distributed within the PLGA matrix, allowing for effective stress transfer and resulting in optimal reinforcement. However, the clustering of TOCNs can lead to points of stress concentration, which diminishes the overall tensile strength. Additionally, higher concentrations may hinder the effective transfer of stress from the PLGA matrix to the nanofillers.



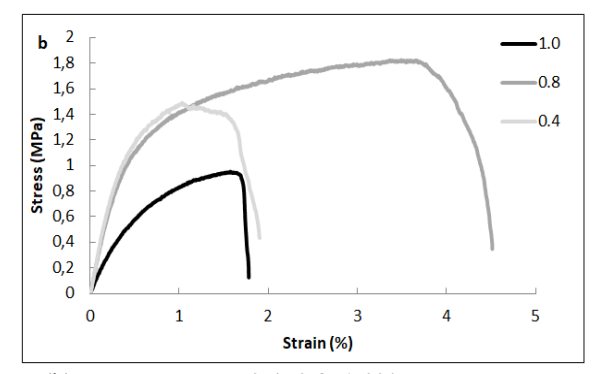


Figure 7: Tensile strength of (a) PLGA, (b) PLGA-TOCNs 0.4, 0.8, 1.0%

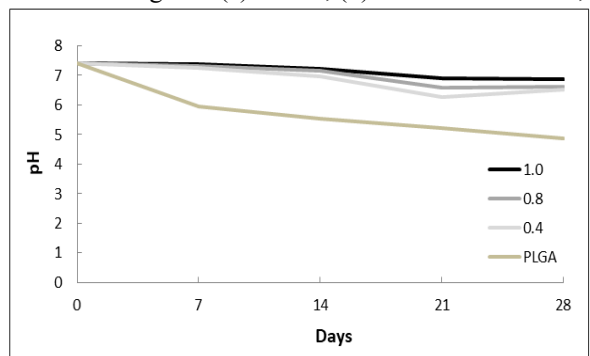


Figure 8: pH measurement of PLGA and PLGA-TOCNs (0.4, 0.8, 1.0%) for 28 days

pH measurement and degradation rate

The pH of all the membranes starts near neutral (pH 7.4) on day 0 and decreases gradually over 28 days (Fig.8). The PLGA sample shows the steepest decline in pH, indicating more significant acidification or degradation compared to other samples. The PLGA-TOCNs 0.8 and 1.0 membranes demonstrated greater pH stability over 28 days, compared to PLGA and lower TOCNs concentrations (e.g., 0.4%). The data on pH changes and degradation rates provide insights into the degradation mechanisms and the influence of TOCNs incorporation. The decrease in pH is a characteristic feature of PLGA degradation, as the hydrolysis of the ester bonds in PLGA produces

acidic by-products (lactic acid and glycolic acid) that lower the pH of the surrounding environment. ^{50,66} The finding that the PLGA sample experiences the most significant drop in pH indicates that it hydrolyzes more quickly than the PLGA-TOCNs membranes.

The integration of TOCNs into PLGA had a substantial impact on the degradation characteristics of the composite membranes. Over a 28-day period, the average degradation rates for PLGA, PLGA-TOCNs at 0.4%, 0.8%, and 1.0% were found to be 36.63%, 28.92%, 19.96%, and 17.31%, respectively. Statistical evaluation via one-way ANOVA followed by Tukey's post hoc test (p < 0.05) indicated that the degradation rate of

unmodified PLGA was significantly greater than that of both PLGA-TOCNs 0.8% and 1.0%. This pattern implies that a higher concentration of TOCNs effectively reduces the degradation rate. Several factors may play a role in this stabilization phenomenon. First, PLGA-TOCNs 0.8% and 1.0% demonstrated a smaller pore size and lower pore volume when compared to both PLGA and PLGA-TOCNs 0.4%, which likely limits water absorption and hydrolytic chain scission. Additionally, the carboxylate groups on the surface of the TOCNs might provide a buffering effect, lessening the acidification that is usually associated with degradation products of PLGA, such as lactic and acids. 53,67 glycolic The рН measurements corroborate this observation, with PLGA exhibiting a more pronounced pH decrease over 28 days, while PLGA-TOCNs 0.8% and 1.0% displayed enhanced pH stability. This buffering capability, combined with decreased porosity, enhances structural integrity and regulates biodegradation, which are essential for biomedical uses such as scaffolds and membranes. These findings are consistent with earlier studies indicating that the incorporation of nanocellulose into biodegradable polymers not only improves mechanical strength, but also influences degradation rates.⁶⁸⁻⁷⁰

CONCLUSION

The results of the study indicate that the utilization of nanofibers produced from OPEFB by TEMPO-mediated oxidation changes the morphology of the PLGA membrane, leading to the formation of a more porous structure, which is stimulated by cross-linking between nanocellulose (TOCNs) and PLGA polymers. This study provides an overview of the utilization of non-wood fibers from OPEFB waste that can be used to develop functional membrane scaffolds or membrane enhancer, starting from PLGA membranes, which are widely used for guided bone regeneration applications. However, this study has its limitations, as it does not include in vivo tests of the material, and it noteworthy that the behavior of the membranes in clinical application could be different. Therefore, the material's biocompatibility and long-term stability need further investigation.

ACKNOWLEDGEMENT: This study was conducted with financial assistance from Universitas Padjadjaran, Bandung. This study was supported by the Centre for Biomaterials Research and Studies, Faculty of Dentistry, Universitas

Padjadjaran. Sincere appreciation is expressed to the Integrated Laboratory of Bioproducts, National Research and Innovation Agency (BRIN), Cibinong, Republic of Indonesia, for providing XRD analysis; and to the Laboratory of the Center for Sustainable Forest Management, Ministry of Forestry, Bogor, Republic of Indonesia, for providing surface area analysis.

REFERENCES

¹ S. Kagozar, P. Milan, F. Baino and M. Mozafari, in "Nanoengineered Biomaterials for Regenerative Medicine", edited by M. Mozafari, J. Rajadas and D. Kaplan, Elsevier Inc., 2019, pp. 13–38, https://doi.org/10.1016/B978-0-12-813355-2.00002-8

² Y. D. Rakhmatia, Y. Ayukawa, A. Furuhashi and K. Koyano, *J. Prosthodont. Res.*, 57, 3 (2013), https://doi.org/10.1016/j.jpor.2012.12.001

³ M. Abtahi, M. Mohammadi, M. Fathi, F. Yazdian and F. Ganji, *ACS Mater.*, 3, 279 (2023), https://doi.org/10.1021/acsmaterialsau.3c00013

⁴ F. Gao, L. Zhang, Y. Liu, Y. Ma, X. Lu *et al.*, *Polymers* (*Basel*), **14**, 871 (2022), https://doi.org/10.3390/polym14050871

⁵ Y. Yang, Q. Yu, W. Hu, Y. Zhao, X. Bai *et al.*, *Front. Bioeng. Biotechnol.*, **10**, 921576 (2022), https://doi.org/10.3389/fbioe.2022.921576

⁶ X. Chen, X. Jin, M. Zhang, L. Xu and W. Tang, Metals, 12, 2074 (2022), https://doi.org/10.3390/met12122074

⁷ H. Ali, A. Khalid, M. Saleem, M. Munir, M. S. Qureshi *et al.*, *Biomed. Mater. Eng.*, **29**, 012010 (2024), https://doi.org/10.1088/2057-1976/ad1e75

⁸ W. Florjanski, A. Massler, M. Orzechowska, M. Rosowski, T. Smektala *et al.*, *Polymers (Basel)*, **11**, 782 (2019), https://doi.org/10.3390/polym11050782

S. Takallu, C. Han, B. Nair, A. Bogue, O. Sahin *et al.*, *ACS Infect. Dis.*, **10**, 1 (2024), https://doi.org/10.1021/acsinfecdis.3c00568

Y. Wang, Q. Yu, W. Hu, X. Bai and J. Gao, Front. Bioeng. Biotechnol., 10, 921576 (2022), https://doi.org/10.3389/fbioe.2022.921576

¹¹ J. Ren, Z. Li, X. Bai, Y. Liu and Y. Zhang, *Int. J. Mol. Sci.*, **23**, 14987 (2022), https://doi.org/10.3390/ijms232314987

12 R. Moorehead, S. Song, Z. Wu and M. Qian, *Polymers*, **15**, 3355 (2023), https://doi.org/10.3390/polym15163355

¹³ R. Bizelli, R. Martins, P. Batista, A. Santos, M. de Souza *et al.*, *Biomimetics*, **9**, 431 (2024), https://doi.org/10.3390/biomimetics9070431

Y. D. Rakhmatia, Y. Ayukawa, Y. Jinno, A. Furuhashi and K. Koyano, *Odontology*, **105**, 408 (2017), https://doi.org/10.1007/s10266-017-0298-1

¹⁵ Y. D. Rakhmatia, Y. Ayukawa, I. Atsuta, A. Furuhashi and K. Koyano, *Odontology*, **103**, 218 (2015), https://doi.org/10.1007/s10266-014-0151-8

- B. Solomon, A. Banerjee and P. Mishra, *Appl. Sci.*,
 12, 1042 (2022), https://doi.org/10.3390/app12031042
- ¹⁷ Y. D. Rakhmatia, Y. Ayukawa, A. Furuhashi and K. Koyano, *Int. J. Oral Maxillofac. Implants*, **29**, 826 (2014), https://doi.org/10.11607/jomi.3219
- ¹⁸ T. Urban, A. Csiszar, B. Szabo, D. Nyul, E. Varga *et al.*, Preprint (2024), https://publicatio.bibl.uszeged.hu/31190/1/Urban.pdf
- ¹⁹ J. Huang, Y. Zhao and H. Liu, *Metals*, **12**, 2074 (2022), https://doi.org/10.3390/met12122074
- S. Jin, X. Xia, J. Huang, C. Yuan, Y. Zuo et al., Acta Biomater., 127, 56 (2021), https://doi.org/10.1016/j.actbio.2021.03.067
- ²¹ H. Zhang, Y. Moriyama, Y. Ayukawa, Y. D. Rakhmatia, Y. Tomita *et al.*, *Odontology*, **107**, 37 (2019), https://doi.org/10.1007/s10266-018-0376-z
- ²² H. Namanloo, B. Pourabbas, M. Jahanshahi and M. R. Naimi-Jamal, *J. Biomed. Mater. Res.*, **2022**, 2489399 (2022), https://doi.org/10.1155/2022/2489399
- ²³ N. Doost, Z. Ahmad, M. Farhadi, M. Taghizadeh, A. Raza *et al.*, *Polym. Adv. Technol.*, **35**, e6263 (2024), https://doi.org/10.1002/pat.6263
- N. Hastuti, K. Kanomata and T. Kitaoka, *IOP Conf. Ser. Mater. Sci. Eng.*, 935, 012051 (2020), https://doi.org/10.1088/1757-899X/935/1/012051
- ²⁵ G. Singh, C. Lee, W. Zhang, S. Renneckar, P. J. Vikesland *et al.*, *Water Res.*, **104**, 137 (2016), https://doi.org/10.1016/j.watres.2016.07.073
- ²⁶ A. Isogai, T. Saito and H. Fukuzumi, *Nanoscale*, **3**, 71 (2011), https://doi.org/10.1039/c0nr00583e
- F. Padzil, M. Khalid, M. Khairul, A. Maulana, A. Khalina *et al.*, *Materials*, 13, 1245 (2020), https://doi.org/10.3390/ma13051245
- ²⁸ C. Intharapichai, Doctoral Thesis, Kyoto Institute of Technology, 2020, https://open.lib.kit.go.in/raps/stars//10212/2578/D1

https://opac.lib.kit.ac.jp/repo/repository/10212/2578/D1-0968 h1.pdf

- ²⁹ Y. Amanda, E. Safitri, E. Rachmawati and E. Rahmawati, *IOP Conf. Ser. Earth Environ. Sci.*, **891**, 012016 (2021), https://doi.org/10.1088/1755-1315/891/1/012016
- A. M. B. Khalid, Master's Thesis, Universiti Sains Malaysia,
 http://eprints.usm.my/60085/1/AINA%20MARDHIA%2

0BINTI%20KHALID%20-%20TESIS%20cut.pdf

31 A. M. Salleh, S. M. Lee, D. Mohamad, A. Yusof, N.

Anuar *et al.*, *Heliyon*, **10**, e06855 (2024), https://doi.org/10.1016/j.heliyon.2024.e06855

32 N. Hastuti, K. Kanomata and T. Kitaoka, *IOP Conf.*

- Ser. Earth Environ. Sci., **359**, 012008 (2019), https://doi.org/10.1088/1755-1315/359/1/012008
- ³³ N. Hastuti, K. Kanomata and T. Kitaoka, *J. Polym. Environ.*, **26**, 3698 (2018), https://doi.org/10.1007/s10924-018-1248-x
- L. Segal, J. J. Creely, A. E. Martin and C. M. Conrad, *Text. Res. J.*, 29, 786 (1959), https://doi.org/10.1177/004051755902901003

- ³⁵ E. Lagreca, V. Onesto, C. D. Natale, S. L. Manna and P. A. Netti, *Prog. Biomater.*, **15**, 153 (2020)
- ³⁶ A. P. A. de Carvalho, R. Értola and C. A. Conte-Junior, *Int. J. Pharm.*, **652**, 123851 (2024), https://doi.org/10.1016/j.ijpharm.2024.123851
- ³⁷ D. Klemm, F. Kramer, S. Moritz, T. Lindstrom, M. Ankerfors *et al.*, *Angew. Chem. Int. Ed.*, **50**, 5438 (2011), https://doi.org/10.1002/anie.201001273
- ³⁸ A. B. Rashid, M. Haque, S. M. M. Islam and K. M. R. U. Labib, *Heliyon*, **10**, e24692 (2024), https://doi.org/10.1016/j.heliyon.2024.e24692
- ³⁹ X. Tang, B. Wang, Y. Gao, W. Li and S. Lu, J.

Phys.: Conf. Ser., 2845, 1 (2024),

https://doi.org/10.1088/1742-6596/2845/1/012019

- L. Kong, D. Zhang, Z. Shao, B. Han, Y. Lv et al.,
 Desalination, 332, 117 (2014),
 https://doi.org/10.1016/j.desal.2013.11.005
- 41 R. Kuramae, T. Saito and A. Isogai, *React. Funct. Polym.*, **85**, 126 (2014), https://doi.org/10.1016/j.reactfunctpolym.2014.06.011
- ⁴² A. A. Shefa, M. Park, J. G. Gwon and B. T. Lee, *Mater. Design*, **224**, 111404 (2022), https://doi.org/10.1016/j.matdes.2022.111404
- ⁴³ N. Hastuti, D. A. Indrawan, K. Kanomata and T. Kitaoka, *Cellulose Chem. Technol.*, **57**, 945 (2023), https://doi.org/10.35812/CelluloseChemTechnol.2023.57 .83
- ⁴⁴ T. Saito and A. Isogai, *Carbohyd. Polym.*, **61**, 183 (2005), https://doi.org/10.1016/j.carbpol.2005.04.009
- ⁴⁵ R. Zhao, E. Songfeng, D. Ning, Q. Ma, B. Geng *et al.*, *Compos. Commun.*, **35**, 101322 (2022), https://doi.org/10.1016/j.coco.2022.101322
- ⁴⁶ R. Sun, J. Zhu, H. Wu, S. Wang, W. Li *et al.*, *Int. J. Biol. Macromol.*, **180**, 510 (2021), https://doi.org/10.1016/j.ijbiomac.2021.03.092
- 47 Y. Sue, B. Zhang, R. Sun, W. Liu, Q. Zhu *et al.*,
 Drug Deliv., 28, 1397 (2021),
 https://doi.org/10.1080/10717544.2021.1938756
- ⁴⁸ N. Dey, S. Bhardwaj and P. K. Maji, *RSC Sustain.*, (2025),
- https://pubs.rsc.org/en/content/articlepdf/2025/su/d5su00 142k
- ⁴⁹ V. Raju, R. Revathiswaran and K. S. Subramanian, *Sci. Rep.*, **13**, 18722 (2023), https://doi.org/10.1038/s41598-023-45766-0
- ⁵⁰ N. Han, S. H. Weon, J. Han, J. E. Cha and S. H. Lee, *Biomacromolecules*, (2025),
- https://pubs.acs.org/doi/abs/10.1021/acs.biomac.4c01770 M. Manimaran and M. N. Norizan, *Phys. Sci. Rev.*, **10**, (2025),
- $https://www.degruyterbrill.com/document/doi/10.1515/p\\ sr-2024-0025$
- D. Shen, G. Liu, J. Zhao, J. Xue, S. Guan *et al.*, *J. Anal. Appl. Pyrol.*, 112, 56 (2015), https://doi.org/10.1016/j.jaap.2015.02.022
- ⁵³ H. K. Makadia and S. J. Siegel, *Polymers (Basel)*, **3**, 1377 (2011), https://doi.org/10.3390/polym3031377

- ⁵⁴ R. A. Jain, *Biomaterials*, **21**, 2475 (2000), https://doi.org/10.1016/S0142-9612(00)00115-0
- ⁵⁵ Y. Wu, Y. Wang, F. Wang, Y. Huang and J. He, *Polymers*, **14**, 4756 (2022), https://www.mdpi.com/2073-4360/14/21/4756
- ⁵⁶ T. G. do Nascimento, *Molecules*, **27**, 6959 (2022), https://www.mdpi.com/1420-3049/27/20/6959
- ⁵⁷ A. Tuanchai, *Polymers*, **16**, 1679 (2024), https://www.mdpi.com/2073-4360/16/12/1679
- ⁵⁸ A. Bukhari, *Dose-Response*, **21**, 1 (2023), https://doi.org/10.1177/15593258231152117
- M. E. Culica, A. L. Chibac-Scutaru, V. Melinte and S. Coseri, *Materials*, 13, 2955 (2020), https://www.mdpi.com/1996-1944/13/13/2955
- ⁶⁰ N. Hasan, J. Lee, H. J. Ahn, W. R. Hwang and M. A. Bahar, *Pharmaceutics*, **14**, 22 (2021), https://www.mdpi.com/1999-4923/14/1/22
- M. Kocagöz, Master's Thesis, Izmir Institute of Technology, 2024, https://openaccess.iyte.edu.tr/bitstream/11147/15123/1/1 5123.pdf
- ⁶² R. A. O. Bernal, *Polymers*, **15**, 2037 (2023), https://www.mdpi.com/2073-4360/15/9/2037
- 63 P. H. Maheshwari, R. B. Mathur and T. L. Dhami, *Electrochim. Acta*, **54**, 655 (2008), https://doi.org/10.1016/j.electacta.2008.07.029
- ⁶⁴ F. Wang and Z. Shao, *Ind. Crop. Prod.*, **152**, 112521 (2020), https://doi.org/10.1016/j.indcrop.2020.112521
- 65 H. Fukuzumi, T. Saito, Y. Okita and A. Isogai, *Polym. Degrad. Stab.*, **95**, 1502 (2010), https://doi.org/10.1016/j.polymdegradstab.2010.06.01
- ⁶⁶ A. Gopferich, *Biomaterials*, **17**, 103 (1996), https://doi.org/10.1016/0142-9612(96)85755-3
- 67 R. Tanaka, T. Saito and A. Isogai, *Int. J. Biol. Macromol.*, **51**, 228 (2012), https://doi.org/10.1016/j.ijbiomac.2012.05.016
- ⁶⁸ N. Lin and A. Dufresne, *Eur. Polym. J.*, **59**, 302 (2015), https://doi.org/10.1016/j.eurpolymj.2014.07.025
- ⁶⁹ S. S. Nair, J. Y. Zhu, Y. Deng and A. J. Ragauskas, Sustain. Chem. Process., 2, 23 (2014), https://doi.org/10.1186/s40508-014-0023-0
- A. N. Frone, D. M. Panaitescu, I. Chiulan, C. A. Nicolae, Z. Vuluga *et al.*, *J. Mater. Sci.*, **51**, 9771 (2016), https://doi.org/10.1007/s10853-016-0212-1